European Journal of Pharmaceutics and Biopharmaceutics 71 (2009) 55–63

Contents lists available at ScienceDirect

European Journal of Pharmaceutics and Biopharmaceutics

journal homepage: www.elsevier.com/locate/ejpb

Research paper

Rheology and molecular mobility of amorphous blends of citric acid and paracetamol

Pekka Hoppu [a,*], Sami Hietala [b], Staffan Schantz [c], Anne Mari Juppo [d]

[a] Division of Pharmaceutical Technology, University of Helsinki, Finland
[b] Department of Chemistry, University of Helsinki, Finland
[c] AstraZeneca R&D, Mölndal, Sweden
[d] Division of Pharmaceutical Technology, Industrial Pharmacy, University of Helsinki, Finland

ARTICLE INFO

Article history:
Received 19 February 2008
Accepted in revised form 29 June 2008
Available online 8 July 2008

Keywords:
Amorphous
Rheology
Solid dispersion
Molecular mobility
Physical stability

ABSTRACT

The aim of this study was to investigate the rheological properties, molecular mobility and crystallization tendency of pure citric acid and paracetamol or blends of them. Amorphous samples were produced by ethanol-evaporation or by melt-quenching. Enthalpy recovery, glass fragility and heat capacity were determined by differential scanning calorimetry (DSC). Other physical characterization methods were rheology and the crystallization tendency using X-ray powder diffraction (XRPD) and DSC. All the samples behaved as Newtonian liquids and they were fragile glasses. The 50/50 (w/w,%) blend had good physical stability upon consecutive shearing regardless of the preparation method. All the samples were stable for at least one year in dry conditions at −20 °C. The melt-produced blends containing 25% or 50% paracetamol were stable at least two years in dry ambient conditions. The good physical stability at ambient temperature cannot be explained by molecular mobility because molecular mobility of the model material is less than 100 s in ambient conditions. Thus other factors, such as the thermodynamic and crystallization driving forces or formation of degradation products, must determine the physical stability of the blends. The composition and processing method have an impact on the physical stability of the sample.

1. Introduction

In the pharmaceutical literature, amorphous drugs or amorphous blends studied nowadays usually have a higher glass transition temperature (T_g) than ambient temperature. This is due to the fact that amorphous materials having a T_g lower than the ambient temperature are hard to produce. Also it is hard for them to remain amorphous [1]. One explanation for the poor physical stability of low T_g amorphous materials is fast molecular mobility, because molecular mobility is closely related to the physical stability of an amorphous state. Molecular mobility of amorphous materials at T_g is about 100 s, and much less at temperatures higher than T_g [2]. Molecular mobility is the combination of different molecular movements, such as the translational and rotational motions of molecules. Translational motion ceases at temperatures lower than T_g but there is still some restricted rotational and vibrational mobility. However, the crystallization tendency is not always related to the molecular mobility of small glass formers. Other important factors such as molecular interactions and thermodynamic properties may be involved [3–6]. Similarly, other properties of the amorphous state, including chemical reactivity in glass, are not dependent on molecular mobility alone, but they may be affected by other factors which are not understood [7]. In addition, relaxation time is reported to change as a function of annealing time [8,9] and the way the sample is handled may also change molecular mobility [10].

Similarly, lowered viscosity can be connected with the increased molecular mobility of the amorphous system. Viscosity is an important physical parameter of amorphous materials since it is directly related to processability. Still, only a few papers have dealt with the viscosity of amorphous drugs [11–13]. Viscosity contributes to material properties like stickiness, adhesion and softness [14]. Usually, the viscosity of the glassy material is considered to be approximately 10^{12} Pa s, but it may vary between different systems [15].

Since the development of a new chemical entity has led to problems in crystallization, because of the structural complexity of new drugs [16], this will increase the amount of amorphous drugs in formulation development. Because some amorphous drugs will have a T_g lower than ambient temperature, there is a need for a physically stable and sticky amorphous model drug system for large-scale processing studies. Further processing of materials with

* Corresponding author. Division of Pharmaceutical Technology, Faculty of Pharmacy, P.O. Box 56, 00014 Helsinki, University of Helsinki, Finland. Tel.: +358 9 19159674; fax: +358 9 19159144.
E-mail address: pekka.hoppu@helsinki.fi (P. Hoppu).

0939-6411/$ - see front matter © 2008 Elsevier B.V. All rights reserved.
doi:10.1016/j.ejpb.2008.06.029

List of symbols and abbreviations

KWW	Kohlrausch–Williams–Watts equation
τ^{kww}	mean molecular relaxation time constant (KWW)
β	mean relaxation time distribution constant (KWW)
ϕ	relaxation function
ΔH	enthalpy recovery
ΔH_∞	maximum enthalpy recovery
C_p	specific heat capacity
ΔC_p	change of specific heat capacity at T_g
T_g	glass transition
T_g^o	$T_g$onset (extrapolated)
T_g^{mid}	$T_g$midpoint
T	temperature
t	storage time
AGV	Adam–Gibbs–Vogel
τ^0	initial relaxation time
τ_0	pre-exponential factor (approximately similar to vibrational lifetimes 10^{-14} s)
x	crystalline
g	glassy
l	liquid
γ	related to C_p ratio of the crystalline (x) and glassy (g) material at T_g
D	strength parameter
T_0	ideal glass transition temperature where relaxation times approach infinity
T_k	Kauzmann temperature
T_f	fictive temperature, temperature where a property of a non-equilibrium state (enthalpy/entropy) corresponds to an equilibrium state
T_f^0	initial fictive temperature
DSC	differential scanning calorimetry
MDSC	modulating DSC
R	gas constant
η^*	complex viscosity
G'	storage modulus
G''	loss modulus
ω	angular velocity
E_a	flow activation energy
η	viscosity
VTF	Vogel–Tamman–Fulcher
A	material parameter
τ	molecular relaxation time
XRPD	X-ray powder diffraction
HPLC	high performance liquid chromatography
DEA	dielectric analysis
GC	gas chromatography
RH	relative humidity
PARA	paracetamol
CAA	citric acid anhydrate
CAM	citric acid monohydrate
PARA25	sample containing 25% (w/w) of PARA
PARA50	sample containing 50% (w/w) of PARA
PARA75	sample containing 75% (w/w) of PARA
EtOH	ethanol
wt/%	weight% is the same as w/w (%)

low-T_g to the solid dosage form is difficult due to the sticky nature [17]. Citric acid and paracetamol blends have been studied earlier [18] and recently we characterized this blend using modern analytical methods [19]. At room temperature, it was shown to be physically stable long enough to be a model system with low-T_g. The aim of this work was to study rheology, physical stability and molecular mobility properties of pure citric acid and paracetamol or blends of them prepared with different methods. The citric acid and paracetamol blend will work as a model material in processing studies in the future, imitating a physically stable amorphous sticky drug. This system can be used instead of a true drug substance of interest, which is sticky, amorphous, highly potent and expensive.

2. Materials and methods

2.1. Materials and design of experiment

2.1.1. Sample preparation

The materials and preparation of melt-quenched samples have been previously described in detail [19]. The sample size in melt-quenching was 50 g. Factors used in the design of the experiment were: the melting temperature, the melting time at constant temperature and the composition of the blend. Compositions were melted in a thermostated electric heating reactor, and the hot melt was cooled down in aluminum pans floating on liquid nitrogen.

The compositions used in ethanol-evaporation were pure citric acid, PARA25 and PARA50 (paracetamol%, w/w). The sample size used was 6.0 g. The samples were dissolved to 15 g of 96% (V/V) ethanol (Altia, Rajamäki, Finland) with a thermostated magnet stirrer (+50 °C). The solution was poured into an aluminum pan on a thermostated hot plate (110 ± 10 °C) with vacuum (at the end of drying the vacuum used was 100 mbar). The samples were held under these conditions for 30 min (residual weight approximately 4–10% w/w), after which they were set in a vacuum oven (110 °C, 40 mbar). The samples were kept in the oven as long as the residual weight increase was less than 0.5% (w/w) as calculated from the total weight of added dry powder.

2.2. Rheology

Viscosity measurements were made from selected melt-produced samples (all duplicates and samples 0–6–179 and 75–6–186 [amount of PARA (%, w/w) – melting time (min) – melting temperature (°C)]). All ethanol-evaporated samples were measured. Rheological measurements were carried out using a TA Instruments AR2000 controlled stress rheometer (TA instruments, DE, USA). A parallel plate configuration with a 20 mm diameter steel plate, and a gap setting of 1.5 mm was used as a measuring setup. Measurements were made at temperatures between 40 and 100 °C (n = 2-4). For dynamic measurements, the linear region was established by performing a strain sweep, while frequency sweeps were made typically in the frequency range of 100–0.01 rad/s. In steady shear-flow measurements, shear rates from 0.1 to 500 1/s were applied in a controlled rate mode.

The zero-shear viscosities for calculations were taken from the values of complex viscosity ($\eta^* = [(G')^2 + (G'')^2]^{1/2}/\omega$) at low-frequencies. The apparent melt-flow activation energy was determined from the temperature dependency according to the Arrhenius equation

$$\eta = Ae^{\frac{E_a}{RT}}, \quad (1)$$

where η is the viscosity (Pa s), A is a constant, E_a is the apparent flow energy (J/mol), R is the gas constant (J mol^{-1} K^{-1}) and T is the temperature (K). Parameters were also determined using the Vogel–Tamman–Fulcher (VTF) equation

$$\eta = Ae^{\frac{DT_0}{T-T_0}}, \quad (2)$$

where T_0 is the transition temperature and A and D are material parameters. The temperature T_0 corresponds to ideal glass transition temperature where viscosity and relaxation times approach infinity. T_0 is typically mentioned to be quite near the T_k (Kauzmann temperature) where all the molecular motion in the glass vanishes. The "strength parameter" D indicates the extent of deviation from Arrhenius' law and it may be used in describing the fragility of the liquids. Typically, D would be below 10 for fragile liquids and 30 to infinity for very strong liquids [20–22]. Because viscosity (η) relates to molecular relaxation time (τ), the VTF equation can be presented as Eq. (3) below [2,13]. With the help of this relationship, τ can be calculated above T_g. In Eq. (3), τ_0 is the pre-exponential factor, which is usually of a similar order as vibrational lifetimes 10^{-14} s.

$$\tau = \tau_0 e^{\frac{DT_0}{T-T_0}} \quad (3)$$

2.3. Thermoanalytical characterization

2.3.1. Glass transition temperature

The glass transition temperature (T_g) of the samples was measured 12 h after the evaporation of ethanol with a Mettler DSC823^e (Mettler-Toledo AG, Greifensee, Switzerland) with Julabo FT900 intercooler (Seelbach, Black Forest, Germany) ($n = 3$). Onset (T_g^o) (extrapolated) and midpoint (T_g^{mid}) values were determined. The nitrogen gas flow during measurements was 50 ml/min. The sample size was 9 ± 1 mg using 40 μl aluminum pans with a pinhole. The temperature ranged from −40 to +100 °C. Two scans were made for each sample at the same temperature range. The sample was held for 10 min at −40 °C to stabilize the temperature before scans. The heating rate was 10 °C/min and the cooling rate approximately 25 °C/min. An analysis of melt-quenched samples has been presented previously [19].

2.3.2. Enthalpic relaxation

Enthalpic relaxation was measured using DSC. Sample size was 9 ± 0.5 mg and the pan was hermetically sealed ($n = 3$). Pure PARA and CAA samples were melt in-situ. The temperature was 5 °C higher than the reported melting temperature and the melting time was 5 min, after which the samples were cooled to −40 °C at a cooling rate of 10 °C/min. Chemical purity of in-situ samples was more than 98% measured with HPLC (Method presented elsewhere [19]). In addition, the bulk samples of PARA50 ethanol-produced and PARA50 melt-produced materials were measured.

The measured samples were first cooled to −40 °C, after which the sample was heated to 40 °C and cooled again to destroy the thermal history. The sample was heated from −40 °C to storage temperature and held there for a specific time. The relaxation times were 1, 2, 3, 4, 8, 16 and 24 h, after which the sample was cooled again to −40 °C. The sample was scanned twice from −40 to 40 °C to measure enthalpy recovery in the first scan (ΔH) and to check the total enthalpy recovery in the second scan. Heating and cooling rates were 10 °C/min and relaxation temperatures were 10 or 20 °C lower than T_g (accuracy ±1 °C). The area obtained at time ($t = 0$) was subtracted from all the other annealing time points as recommended [1]. The Kohlrausch–Williams–Watts (KWW) equation Eq. (4) was used to define the mean molecular relaxation time constant (τ^{kww}) and mean relaxation time distribution constant (β). Maximum enthalpy recovery (ΔH_∞) was calculated as below Eq. (5) where the measured heat capacity change (ΔC_p) at T_g is needed. The storage temperature is (T) and the storage time is (t).

$$\phi = 1 - \left(\frac{\Delta H}{\Delta H_\infty}\right) = \exp\left[-\left(\frac{t}{\tau^{kww}}\right)^\beta\right] \quad (4)$$

$$\Delta H_\infty = (T_g - T)\Delta C_p \quad (5)$$

2.3.3. Heating-rate dependence

Fragility parameters (D and T_0) were defined by the heating rate dependence method [9,23] using a normal DSC mode ($n = 3$). Measurements were made similarly to those presented in the literature [9] except that samples were cooled at a 40 °C (not 50 °C as they did) lower temperature than T_g because of intercooler inefficiency. T_g midpoints (T_g^{mid}) were used to define fragility and activation enthalpies using a normal DSC mode. Heating and cooling rates were similar: 2, 5, 10, 15, and 20 °C/min. Sample size for all the measurements was 9 mg.

2.3.4. Heat capacity measurement

The specific heat capacity (C_p) was measured using the TOPEM mode (TOPEM is a modulating DSC of Mettler-Toledo) ($n = 5$). The thermal history of samples was destroyed before measurement, as in the enthalpic relaxation measurements. Samples were scanned at a temperature ranging from −20 to 40 °C with a heating rate of 1 °C/min, amplitude 0.5 °C and frequency variation of 15–30 s. C_p of crystalline blends were measured from crystalline starting materials weighed directly in the DSC pan in the right ratio.

2.3.5. Time-dependent structural relaxation and initial relaxation time

The Adam–Gibbs–Vogel (AGV) theory is related to the glass relaxation controlled by configurational entropy and activation energy [24]. The AGV equation is often presented as in Eq. (6) [25]. Mao et al. [26] presented a method to calculate the time-dependence of molecular mobility Eqs. 6,7 in which the annealing time of a compound is combined with the AGV theory; we used the same method. In Eq. (6), τ_0 is the pre-exponential factor which is usually of a similar order as vibrational lifetimes 10^{-14} s. The fictive temperature (T_f) Eq. (7) is presented as a following function that is combined with the normal AGV function, and τ is dependent on the change in the T_f. T is the annealing temperature and ΔH the enthalpy relaxed during time as in the KWW equation. Parameter γ is related to the C_p ratio of the crystalline and glassy material at T_g. Superscripts of C_p are liquid (l), glass (g) and crystal (x). In the modified AGV equation Eq. (8), the initial relaxation time (τ^0) was calculated similarly to Mao et al. [9].

$$\tau = \tau_0 \exp\left(\frac{DT_0}{T\left(1 - \frac{T_0}{T_f}\right)}\right) \quad (6)$$

$$T_f = T_f^0 \exp\left(-\frac{\gamma \cdot \Delta H}{\Delta C_p \cdot T_g}\right), \quad T_f^0 = T_g^\gamma \cdot T^{(1-\gamma)} \quad (7)$$

$$\tau^0 = \tau_0 \exp\left(\frac{DT_0}{T - T_0\left(\frac{T}{T_g}\right)^\gamma}\right), \quad \gamma = \left(\frac{C_p^l - C_p^g}{C_p^l - C_p^x}\right)_{T_g} \quad (8)$$

2.4. Other characterization methods

Analysis of the residual ethanol amount was done according to the method and equipment of Klick and Sköld [27]. X-ray powder diffraction (XRPD), Fourier transform infrared microscopy (FT-IR), Karl Fischer titration and aging study (samples were stored at 3% and 43% RH) were done in similar settings as previously described in ambient conditions [19]. The chemical stability of samples was investigated using HPLC (Thermo Separation Products, San Jose, CA, USA) equipped with a UV–vis detector using wavelengths 215 nm for CAA and 245 nm for PARA (model FOCUS, San Jose, CA, USA) [19]. The eluent used was composed of 96% (V/V) water

with 0.1% (V/V) trifluoroacetic acid at pH 2.1 and 4% (V/V) of acetonitril. In addition, samples of enthalpic relaxation study were stored in dry silica at −20 °C for one year, after which the samples were measured with a DSC to check the physical stability of the samples.

3. Results and discussion

3.1. Ethanol-evaporated samples

Amorphous samples were possible to be produce by ethanol-evaporation up to the 50/50 (w/w) blend. Samples containing 75% or more PARA started to crystallize during ethanol-evaporation. A large amount of PARA in the sample eased up the ethanol-evaporation process. Moisture content of dry EtOH samples varied from 0.5% to 0.8% (w/w) in the Karl Fischer titration. The ethanol amount was less than 200 ppm in all the dry samples measured by GC.

If a high amount of residual solvent was captured in the sample (i.e. 5% or more), all the ethanol samples started to crystallize in 24 h (3% RH) due to inefficient ethanol-evaporation. This is the result of residual solvents of ethanol and water in the sample, which dramatically increase the crystallization rate as compared with the pure solvents [28]. Well-dried samples, having less than 1% of water, crystallized much more slowly although the water amount in the samples was almost 10% after two weeks' storage in humid conditions (43% RH) than the samples with high residual solvent content.This is connected to the hydrophilic and hydrophobic nature of the used materials and interaction with molecules. Water is a polar molecule while ethanol has a non-polar alkyl group and a polar hydroxyl group that compete hydrogen bonds and van der Waals interactions between PARA and CAA that will plasticise the sample.

3.2. Comparison of melt-quenched and ethanol-evaporated samples

Degradation of blend samples was similar to that of the samples made by the melt-quenching method as measured by HPLC [19]. The pure ethanol-evaporated CAA sample was estimated to contain less than 10% of the degradation products. In the ethanol-evaporated blends, the purity of PARA was 90–97% (min–max). PARA was less stable in the composition containing 25% PARA. Similarly for pure CAA, the estimated purity was 75–90% in the blends.

Pure CAA was physically more stable when produced by the EtOH method than when produced with melt-quenching. Citric acid monohydrate (CAM) is known to crystallize poorly if no seed crystals are available [29]. In the melt-quenched pure CAA, small crystals were detected right after cooling [19]. These nuclei will grow in storage conditions, increasing the crystallization tendency. In the EtOH method, these nuclei are apparently not formed, which increased physical stability. Under dry conditions, the samples did not crystallize in 52 weeks according to XRPD. However, small crystals were observed with a FT-IR on the surface after 52 weeks in all the samples.

Otherwise, physical stability of melt-quenched samples was better than that of ethanol samples in 3% and 43% RH. A possible reason is the thicker sample layer in the melt-produced samples (5 ± 2 mm) than in the evaporated samples (only 1–2 mm). Water could plasticize the whole sample produced by the EtOH method, favouring crystallization especially in 43% RH [30]. A single glass transition(T_g) was observed in all the DSC scans. None of the ethanol samples crystallized during DSC scans, which was not in accordance with the behaviour of melt samples [19]. Glass transitions of ethanol samples were somewhat lower in comparison with melt-produced bulk samples [19] (Table 1). This was probably due to the small degradation products that did not boil away at 110 °C, as compared with a higher temperature in the melt method (temperature over 170 °C). The existence of volatile degradation products is demonstrated in Hoppu et al. [19], where the CAA/PARA blends melted in-situ in DSC pan had lower T_g when samples were measured without pinhole than when they were measuredwith pinhole in the pan[19]. The volatile degradation products were found to change T_g.

3.3. Rheology

Fig. 1 shows the frequency dependence of the moduli of the different CAA/PARA samples at 80 °C, and Fig. 2 gives the frequency dependence of the moduli of the melt-processed sample at 50 and 80 °C. It can be seen that the samples behave as viscous liquids, loss modulus G″ being significantly higher than storage modulus G′ throughout the measuring frequencies. The frequency dependence of the moduli is somewhat different from what has been observed for indomethacin (T_g^{mid} = 41 °C) [12] where G″ had a clear maxima at varying frequencies at different temperatures between 44 and 56 °C, the maxima shifting to higher frequencies with increasing temperature. No maximum in the loss modulus is observed for

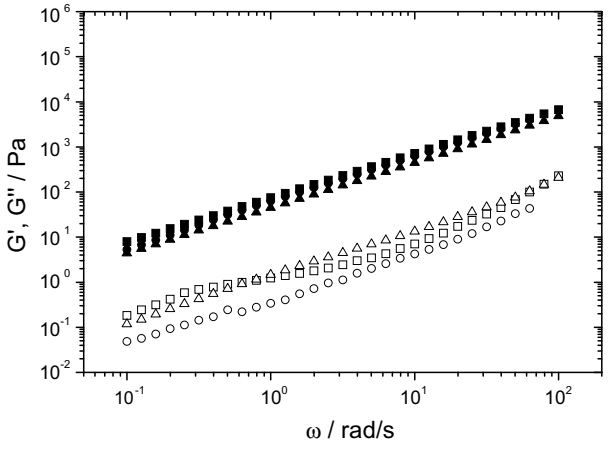

Fig. 1. Dynamic moduli of the ethanol-evaporated samples. CAA (G′Δ, G″▲), PARA25 (G′○, G″●) and PARA50 (G′□, G″■) at 80 °C.

Table 1
The average (avg.) onset (T_g^o) and midpoint (T_g^{mid}) temperature compared with samples produced by bulk melt[a] [19] or ethanol[b] evaporation methods

PARA (w/w,%)	0%[a]		25%[a]		50%[a]		75%[a]		100%[a]		0%[b]		25%[b]		50%[b]	
Parameter	Avg.	±	Avg.	±	Avg.	±	Avg.	±	Avg.	±	Avg.	±	Avg.	±	Avg.	±
T_g^o [°C]	8.7	1.3	8.9	0.8	12.4	1.1	16.8	1.3	-*	-*	-4.7	4.5	0.3	3.8	8.0	4.2
T_g^{mid} [°C]	14.0	1.7	14.7	1.1	17.9	1.5	21.3	0.9	-*	-*	0.1	3.4	6.0	2.4	12.8	2.8

In melt-produced samples the average value is calculated from all the measurements. Ethanol-evaporated samples were measured triplicate (n = 3). The samples are denoted by wt/% of paracetamol (± = SD).
*Crystals, 75% or 100% ethanol samples crystallized during drying.
-Not measured.

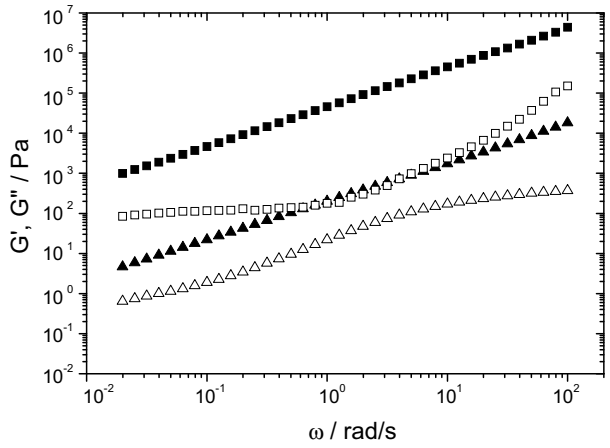

Fig. 2. Dynamic moduli of the melt-processed PARA50 at 50 °C (G′□, G″■) and at 80 °C (G′Δ, G″▲).

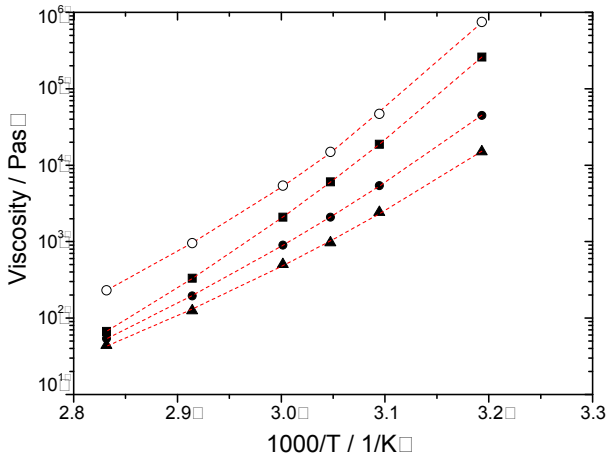

Fig. 3. Reciprocal temperature plot of viscosity of ethanol-evaporated samples, citric acid (▲), 25 wt% (●), 50 wt% (■) PARA/CAA mixture and melt-processed 50 wt% (o) PARA/CAA mixture. Dashed lines are fitted to Eq. (2) between 80 and 40 °C.

the CAA/PARA mixtures and it may be possible that for the CAA/PARA mixtures the measuring temperature is too high for the maxima to be observed at the accessible frequency range.

The composition of the samples affects the viscosity. The viscosity of the blends decreased as the amount of CAA in the composition increased. Citric acid is reported to decrease the shear viscosity of thermoplastic starch even at low-weight proportions [31]. Similarly, lowered viscosity increased the processing possibilities of starch and hindered crystallization of starch due to the strong hydrogen-bond capability of CAA. The rigid molecular structure of PARA, compared with CAA, due to an aromatic ring, may increase the viscosity of the samples. The recorded steady shear viscosities at low-shear rates were on the same level as the complex viscosities. The complex viscosity calculated from the moduli gives nearly constant viscosity and thus samples behave as Newtonian liquids.Additionally, it was found that the melt-processed samples show slightly higher values of moduli and viscosity than the corresponding ethanol-evaporated samples having the same composition. The extrapolated viscosity at the calorimetric T_g^{mid} calculated by the VTF equation was much lower than the often-quoted value of 10^{12} Pa s for glassy materials (Table 2). This behaviour has been observed also for indomethacin [12].

The viscosity increases roughly a decade per each decrease of 10 K in temperature (Fig. 3). The behaviour is not linear with regard to the temperature, and at lower temperatures the viscosity increases faster than at higher temperatures. Similar behaviour has been detected with amorphous salol, α-phenyl-*o*-cresol and *o*-terphenyl [32]. Thus, only apparent activation energies (Table 2) may be calculated from Eq. (1). by using the viscosity values at temperature closest to T_g. As shown in Fig. 3, the deviation from linearity can be fitted using the VTF equation Eq. (2) to access material parameters describing the glass fragility (D^η) and temperature, in which molecular mobility is but insignificant (T_0^η). It can be seen that all samples show deviation from Arrhenius behaviour and the fitting parameters using Eq. (2) are shown in Table 2. For all the samples, values of D^η are close to 10, indicating that the samples can be described as "fragile" according to Angell's classification. The D^η value of ethanol-evaporated blends increased from the pure CAA sample to PARA50, indicating a stronger glass former. These parameters were used to study the molecular mobility.

3.4. Physical stability under shearing

Crystallization proceeded more rapidly under the consecutive shearing than in the desiccator. The melt-produced 25% and 50% PARA blends were amorphous after two years of storage in dry conditions.The melt-processed PARA50 sample shows surprisingly good shear stability up to 80 °C. Upon shearing none of the EtOH samples crystallized during the measurement, although the melt-processed samples with compositions other than 50% tended to crystallize upon heating above 50 °C and upon consecutive shearing. Melt-produced pure CAA samples started to crystallize at 40 °C without any shear. Melt samples containing 25% or 75% PARA started to crystallize under shear but not as rapidly as CAA. The monoclinic PARA crystallized from the sample PARA75. PARA25 formed an amorphous inner part and a crystalline outer part on the steel plate. The outer part was crystalline CAA and the inner part was still amorphous as measured by XRPD and FT-IR. The reason for this kind of behaviour is that the shear strain at the edges of the plate is higher than in the middle.

Table 2
Material parameters calculated from the viscosity data

Citric acid/paracetamol [wt% PARA]	T_0^η [K]	± [K]	D^η	±	E_a,app[c] [kJ/mol]	T_g^{mid} [°C]	± [°C]	Viscosity at calorimetric T_g^{mid} [d] [Pas]
0[b]	218.2	3.2	8.6	2.4	156	0.1	3.4	2.6E + 10
25[b]	210.8	0.6	11.6	0.5	175	6.0	2.4	6.7E + 09
50[b]	213.1	0.4	13.6	0.4	215	12.8	2.8	1.3E + 10
50[a]	241.9	0.6	6.6	0.8	201	14.0	1.0	8.3E + 10

T_0^η and D^η values are based on the VTF fits according to Eq. (2) (The apparent activation energy (E_a) was calculated by Eq. (1)).
[a] Melt-processed.
[b] Ethanol-evaporation.
[c] Using temperatures closer to T_g.
[d] From fit to Eq. (2).

It might be possible that the EtOH method produced a more homogeneous blend without small nuclei, compared with the melting method in which only a glass rod was used in the blending. During shearing, small crystals behaved like nuclei, with small particles stuck around them. This kind of behaviour is observed in dispersion systems [33].

3.5. Thermoanalytical characterization and physical stability

Blends of CAA and PARA had lower T_g than pure PARA, yet the physical stability of PARA was better in the blend than as a pure substance. Thus differences in T_g do not explain good physical stability of the blends when compared to pure PARA. Crystalline heat capacities change linearly, while in the amorphous samples step change is observed at the T_g (Fig. 4). Crystalline PARA and CAA had similar heat capacities as reported earlier [34–36]. Parameters γ for CAA (0.90) and PARA (0.86) were quite similar. This has been presented previously in the literature [5,9].

High ΔC_p is correlated with more stable glass in single-phase amorphous materials [37,38]. This is because of the reduced entropy and the enthalpy of the amorphous system. It correlated well for amorphous PARA and CAA, where change of ΔC_p was higher for CAA than for PARA. In PARA50 blends ΔC_p changes were more related to the heat capacity of pure PARA. One explanation is the composition, in which the mole fraction of PARA was 0.56 and 0.44 for CAA. Change of ΔC_p did not follow exactly the simple additivity of pure materials when ΔC_p should be 0.73 J/g · °C in PARA50. In blends, there are many possibilities for why ΔC_p might change [39]: for instance, the effect of degradation products and possible changes in hydrogen bonding [40]. In the blends, ΔC_p does not approximate the good physical stability of PARA50 blends. The blends had lower ΔC_p than, for example, CAA but still they were physically more stable in comparison with CAA. This might be related to the effect of the aromatic ring on the hydrogen-bond network in the blends [40,41], which might decrease ΔC_p.

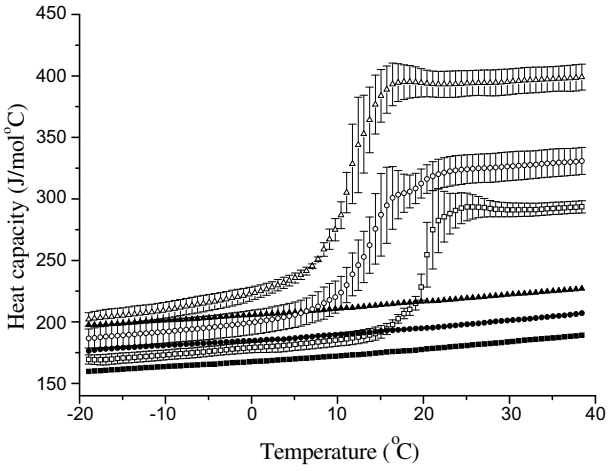

Fig. 4. Heat capacity as a function of temperature for crystalline and amorphous samples. Error bars present the standard deviation ($n = 5$). Open symbols are amorphous samples, and closed symbols are the crystalline material. Symbols: CAA (▲,Δ), PARA (■,□), melt PARA50 (●,○). For crystalline materials $S_{rel\%}$ was approximately 3% ($n = 5$).

CAA and PARA blends can be classified as forming an eutectic mixture at a composition of 50/50 blend (w/w) [42]. The free energy of a mixture is lower than the free energy of pure materials. Theoretically, the 50/50 molar composition of ideal mixtureshould have the lowest free energy of the eutectic mixtures [43]. However, specific interactions between molecules, such as hydrogen bonding as reported earlier [19], may change the molar composition in which the minimum occurs. It is known that the thermodynamic driving force for crystallization is lower for the eutectic mixture than for other compositions [43] and this would agree with the real physical stability of our system.

3.6. Molecular mobility and physical stability

Molecular mobility was attempted to be correlated with the real physical stability of the samples at ambient conditions (25 °C) and at lower temperatures. Relaxation time is reported to estimate physical stability of amorphous samples, but it is not necessarily the only important factor [9]. It has been reported that the crystallization tendency of drugs in the blends may be dependent on the crystallization tendency of pure substances [3]. Because none of the samples crystallised in dry conditions at −20 °C during one year and all the other samples but not 50/50 (or PARA25) blend crystallised at ambient temperature in two years, molecular mobility studies were done at higher temperature than T_g and at lower temperature than T_g.

3.6.1. Enthalpy recovery

If approximately similar annealing temperatures, T_g −20 °C for PARA or T_g −10 °C for CAA and melt PARA50, are compared, it is shown that PARA is the most stable when τ^{kww} is compared (difference in β values) (Table 3). However, melt PARA50 was physically the most stable and pure PARA had the highest crystallization tendency at ambient conditions. It seems that there must also be some other factors besides molecular mobility stabilizing this blend.

Increasing aging time and aging temperature increased the recovery of enthalpy as expected. Mean relaxation times increased as the annealing temperature decreased in all the samples (Fig. 5, Table 3). Pure PARA had the shortest mean relaxation times (τ^{kww}) at T_g −10 °C and at T_g −20 °C. The relaxation time of PARA was different than that reported earlier in the literature [44]. In the previous work, Di Martino et al. [44] could not measure τ^{kww} at a temperature of T_g −10 °C. At T_g −16°C, they reported τ^{kww} to be 32.3 h, and at T_g −22 °C, τ^{kww} was 8.6 h. However, since β values were not similar, the comparison between different samples and studies is difficult [1]. In our study, the τ^{kww} of the CAA samples

Table 3
The heat capacity change (ΔC_p) of in-situ melt-produced samples at the T_g

Composition	T_g^{mid}[c][°C]	ΔC_p[d][J/g · ° C]	T_g −10 °C					T_g −20 °C				
			T_a[°C]	τ^{kww}[h]	±[h]	β	±	T_a[°C]	τ^{kww}[h]	± [h]	β	±
CAA [a]	11.7 ± 0.9	0.84 ± 0.03	2	2.6	0.3	0.5	0.1	−8	64.3	9.9	0.5	0.0
PARA[a]	20.7 ± 0.7	0.64 ± 0.04	11	1.3	0.1	0.7	0.1	1	38.0	4.4	0.5	0.0
PARA50[b]	14.0 ± 1.0	0.70 ± 0.01	4	2.4	0.5	0.8	0.3	-6	64.4	12.3	0.6	0.1

Relaxation times (τ^{kww}) and a distribution of relaxation times (β) at two different annealing temperatures (T_a) according to Eq. (4). ($n = 3$). (± = SD).
[a] In situ melts.
[b] Melt-produced bulk sample.
[c] MDSC ($n = 5$).
[d] Normal DCS mode ($n = 24$).

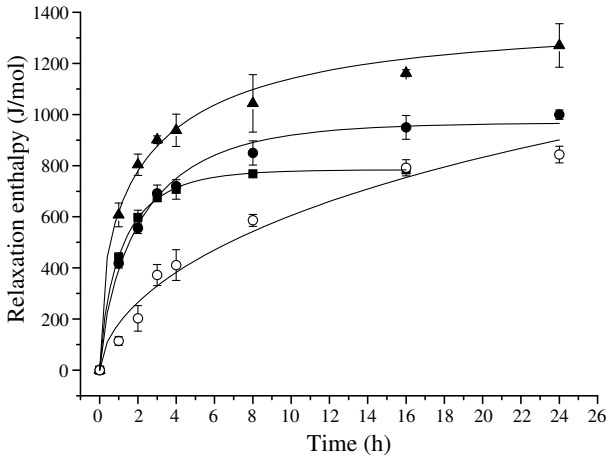

Fig. 5. The relaxation enthalpies of CAA and PARA samples as a function of time at different annealing temperatures. Filled symbols are measured at temperature T_g −10 °C and open at T_g −20 °C. Symbols: In-situ PARA (■), in-situ CAA (▲) and bulk PARA50 melt (●,○). Error bars present the standard deviation in the measurements (n = 3).

was quite similar to that of the PARA50. Ethanol and melt-produced PARA50 samples had similar τ^{kww} at T_g −10 °C and at T_g −20 °C although they had different T_g (data not presented). Enthalpy recovery was more than 0.95 for all the samples at T_g −10 °C. Enthalpy recovery did not achieve the often-demanded 0.8 ($\Delta H/\Delta H_\infty$) relaxation [1] to achieve good reliability of τ^{kww} at T_g −20 °C. The relaxation ratio varied from 0.44 to 0.56 at T_g −20 °C.

3.6.2. Time-dependence of molecular mobility

Because the KWW model gave only mean relaxation time (τ^{KWW}), the change in molecular relaxation time as a function of annealing time was also studied (presented in [26]). The time-dependence of molecular mobility indicated that 100% PARA is physically the most stable glass, if relaxation times are compared although as a pure substance it crystallised rapidly at ambient temperature(Fig. 6). When Eq. (7) was combined with Eq. (6), the relaxation times increased during annealing time in all the samples measured. The highest increase of τ was seen in PARA while melt PARA50 had the slowest increase of τ. PARA had a factor of 42.3 or 27.0 increase of τ after 8 h of annealing at T_g −10 °C or at T_g −20 °C, respectively. In the melt PARA50 τ increased only 11.7 or 5.8 times, respectively. Similarly in CAA, ratios were 16.8 or 14.4, respectively. In all the samples τ increased as the sample relaxed. This kind of behaviour has been reported earlier [26].

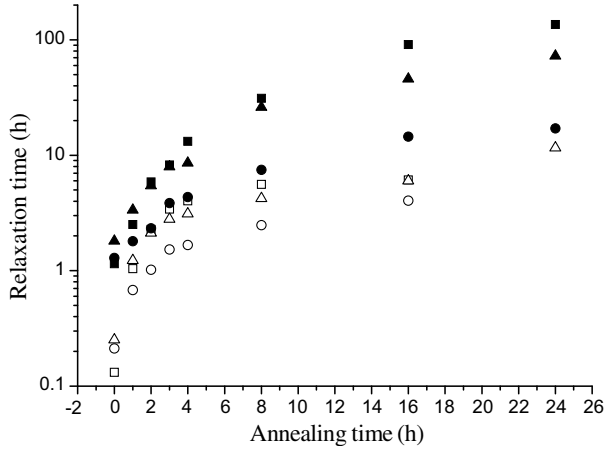

Fig. 6. Time-dependence of molecular mobility (τ) Eqs. (6) and (7) at different annealing temperatures. Calculated from T_g^{mid} values (Table IV). Relaxation time of samples as a function of annealing time. Open symbols are measured at temperature T_g −10 °C and filled at T_g −20 °C. Symbols: In-situ PARA (□, ■), in-situ CAA (Δ,▲) and bulk PARA50 melt (○,●).

3.6.3. Molecular mobility above and below T_g as determined by DSC and rheometer

Relaxation times for freshly prepared, un-annealed samples, as presented in Fig. 7, are calculated using the VTF equation Eq. (3) at a higher temperature than T_g^{mid}, and initial relaxation time (τ^0) using Eq. (8) (modified AGV) at a lower temperature than T_g^{mid}. All the measured samples had approximately similar relaxation times at T_g^{mid}, i.e. approximately 100 s or less, which agrees well with the literature [2].

3.6.3.1. Molecular mobility at temperatures lower than T_g. The modified AGV model Eq. (8) was used to calculate the τ^0 for PARA50. The AGV equation has been used for drug and polymer blends [45], assuming that T_f is the same as T_g. Similarly, for dispersions, γ can be assumed to be 1 if it is difficult to measure crystalline forms. We used the parameters presented in Tables 2 and 4.

Again, molecular mobility calculated by this method correlated poorly with the real physical stability of the samples. Pure PARA showed the highest initial relaxation times (τ^0) (Fig. 7) for freshly prepared glasses although it crystallized most easily at room temperature. Pure CAA had intermediate relaxation times and melt PARA50 had the lowest τ^0 although it was physically the most stable sample at ambient conditions. Differences were similar also when a non-scaled x-axis was used (data not presented).

3.6.3.2. Molecular mobility at temperatures higher than T_g. In temperatures higher than T_g^{mid} (VTF), the viscometry data show lower relaxation times than the DSC data (Fig. 7). This is due to the difference in defined T_0 and D parameters resulting from different methods (Tables 2 and 4). If the x-axis was not scaled (data not presented), PARA50 blends had a higher relaxation time than all the other viscometry-measured samples that was relevant with viscosity (i.e. slow molecular mobility creates high viscosity) (Fig. 3). The VTF equation was calculated with τ_0 as a constant value 10^{-14} s for the viscosity data. Usage of constant τ_0 for the

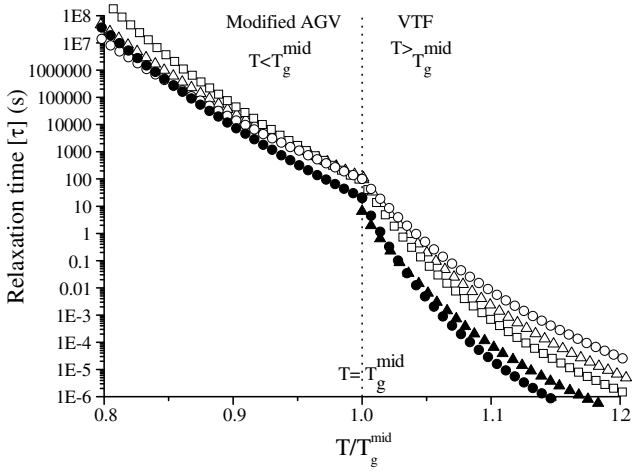

Fig. 7. Molecular relaxation times (τ) as a function of scaled x-axis (T/T_g^{mid}) for freshly prepared glasses from DSC and viscometer data defined by VTF Eq. (3) and initial relaxation time (τ^0) (modified AGV, Eq. (8)). Symbols: viscometer data of EtOH CAA (▲), viscometer data of bulk PARA50 melt (•), DSC data of in-situ melted PARA (□), DSC data of in-situ melted CAA (Δ), DSC data of bulk PARA50 melt (○). Parameters used in calculations are shown in Tables 2 and 4. T_g^{mid} are used in calculations. In VTF equation Eq. (3) τ_0 is constant 10^{-14} s.

Table 4
Fragility parameters (T_0^{hr}, D^{hr}) calculated from heating-rate dependence (n = 3)

CAA/PARA [wt% PARA]	T_g^{mid} [°C]	T_0^{hr} [K]	D^{hr}	ΔC_p [J/g °C]	$\Delta C_p^{x\text{-}l}$ [J/g °C]	γ
CAA[a]	11.7 ± 0.9	215.9 ± 2.7	11.8 ± 0.6	0.82 ± 0.04	0.91 ± 0.03	0.90
PARA[a]	20.7 ± 0.7	231.4 ± 4.7	9.9 ± 0.8	0.64 ± 0.03	0.74 ± 0.02	0.86
PARA50[a]	14.0 ± 1.0	204.5 ± 2.3	14.9 ± 0.6	0.68 ± 0.01	0.75 ± 0.03	0.91
PARA50[b]	10.8 ± 2.5	210.2 ± 5.0	12.9 ± 1.0	0.68 ± 0.03	0.79 ± 0.02	0.86

T_g^{mid} and ΔC_p values measured using MDSC with heating rate 1 °C/min (n = 5) (± = SD).
[a] Melt-processed, CAA and PARA are in situ samples. Melt and EtOH PARA50 are bulk samples.
[b] Ethanol-evaporation.

evaluation of molecular mobility from the viscosity data might not be an ideal method [12].

When a scaled x-axis of the DSC data was used, the samples were in rank order with the real physical stability (Fig. 7) [19]. In addition, the molecular mobility obtained from the DSC data correlated well with the rank order of viscosity presented in Fig. 3. A high viscosity (i.e. low molecular mobility) in the liquid just above the solidification point has been mentioned to be one reason for the formation of glassy state [15]. Differences in viscosity (i.e. molecular mobility) above T_g would explain good physical stability of PARA50 blends compared to other physically stable blends although molecular mobility is high. In the DSC data, PARA had the highest relaxation time in the non-scaled x-axis near T_g^{mid} while melt PARA50 had the highest relaxation time at a higher temperature than 315 K (data not presented). Melt PARA50 had the highest relaxation times and PARA had the lowest when a scaled x-axis was used (Fig. 7). CAA had intermediate relaxation time.

3.6.4. Fragility parameters determined by DSC and rheometer

In all the methods, the blends had higher D values than the pure materials (Tables 2 and 4). There was clear evidence of this in the heating-rate dependence data. Materials with high D value formed glass more easily than materials with low-D value, but this is not usually experimentally confirmed [46]. Fragility values determined using heating-rate dependence method have been found to give higher D parameter values than viscosity data [13], which was also the case in this study. D value seems to be dependent on the measurement method, production method and composition. Degradation products may also have an input in this result. In this study, the difference between T_g and T_0 was approximately 50 °C (Tables 2 and 4). This agrees reasonably well with the literature [47]. T_0 value is estimated to be quite near the temperature at which amorphous pharmaceuticals should be stored to ensure adequate shelf life [47]. Significant differences were observed between measurement methods and reported values in the literature (Tables 2,4,5). The wide distribution in fragility parameters questions the reliability of these parameters expressed without any careful consideration (Table 5). Since, small changes in defined parameters γ, C_p, D, T_g and T_0 affect τ markedly, the parameters used as well as the measurement settings should be clearly presented and measurements should be done carefully [9]. Otherwise, there might be uncertainty in molecular mobility evaluated.

Table 5
Fragility parameters reported in the literature for PARA and citric acid

Method	Sample	D	T_0 [K]	Reference
DSC	CAA	5.6	249	[22]
DSC	CAM[b]	9.6	199	[22]
DSC	CAA	15.0	200.7	[9]
DSC	PARA	7.5	240.5	[48]
DSC	PARA	9.3	236.7	[5]
DEA[a]	PARA	4.9	260.3	[49]

[a] Dielectric analysis.
[b] Citric acid monohydrate.

4. Conclusions

Consecutive shearing tests correlated well with the real physical stability of the samples. In the viscosity studies, the melt-quenched samples crystallized more easily than the ethanol-evaporated samples (EtOH) under consecutive shearing. The exception was the 50/50 blend (w/w), which behaved quite similarly among the different production methods. All the samples behaved as Newtonian liquids and were fragile glass formers according to Angell's classification. The evaluated D value in the Vogel–Tamman–Fulcher (VTF) equation changed with the composition of the blend and the processing method. The viscosity was dependent on the measurement temperature and the composition. The amount of paracetamol in the sample increased the measured viscosity. Slight viscosity differences were observed between samples produced by the melt-quenching or the ethanol-evaporation.

The time-dependent molecular mobility, initial relaxation time and Kohlrauch–William–Watts equations overestimated the physical stability of pure materials compared with the real physical stability where the 50/50 blend was the most stable for at ambient temperature. When the rank order of the samples was compared, molecular mobility calculated by the VTF equation from the DSC (obtained below T_g) and rheometer (obtained above T_g) data correlated with the viscosity measured. At −20 °C all the samples were amorphous after one year storage in dry conditions that correlated well with a long molecular mobility estimated at this temperature. However, the binary system (50/50) of citric acid anhydrate and paracetamol seems to be stable although molecular mobility is relatively high in the supercooled melt in the ambient conditions, i.e. the molecular relaxation time is less than 100 s. Thus, factors other than the molecular mobility are important in the physical stabilization of blends in this composition range. These include structural factors giving rise to thermodynamic driving force and possible degradation products. Degradation products or impurities may increase the stability of the system due to a more complex structure in the blend. A detailed physical property study of pure non-degraded samples will be reported later. The melt-processed 50/50 blend is a good model system in a supercooled liquid state for processing studies due its good physical stability under shearing.

Acknowledgements

We thank AstraZeneca R&D Mölndal for the financial support. The authors are grateful to Agneta Sköld, AstraZeneca R&D and Mölndal for carrying out the GC measurements.

References

[1] B.C. Hancock, S.L. Shamblin, Molecular mobility of amorphous pharmaceuticals determined using differential scanning calorimetry, Therm. Acta 380 (2001) 95–107.
[2] M.D. Ediger, C.A. Angell, S.R. Nagel, Supercooled liquids and glasses, J. Phys. Chem. 100 (1996) 13200–13212.
[3] P. Marsac, H. Konno, L.S. Taylor, A comparison of the physical stability of amorphous felodipine and nifedipine systems, Pharm. Res. 23 (2006) 2306–2316.

[4] H. Konno, L.S. Taylor, Influence of different polymers on the crystallization tendency of molecularly dispersed amorphous felodipine, J. Pharm. Sci. 95 (2006) 2692–2705.
[5] D. Zhou, G.G.Z. Zhang, D. Law, D.J.W. Grant, E.A. Schmitt, Physical stability of amorphous pharmaceuticals: importance of configurational thermodynamic quantities and molecular mobility, J. Pharm. Sci. 91 (2002) 1863–1872.
[6] T. Miyazaki, S. Yoshioka, Y. Aso, T. Kawanishi, Crystallization rate of amorphous nifedipine analogues unrelated to the glass transition temperature, Int. J. Pharm. 336 (2007) 191–195.
[7] S.L. Shamblin, B.C. Hancock, M.J. Pikal, Coupling between chemical reactivity and structural relaxation in pharmaceutical glasses, Pharm. Res. 23 (2006) 2254–2268.
[8] K. Kawakami, M.J. Pikal, Calorimetric investigation of the structural relaxation of amorphous materials: evaluating validity of the methodologies, J. Pharm. Sci. 94 (2005) 948–965.
[9] C. Mao, S.P. Chamarthy, S.R. Byrn, R. Pinal, A calorimetric method to estimate molecular mobility of amorphous solids at relatively low temperatures, Pharm. Res. 23 (2006) 2269–2276.
[10] J. Liu, D.R. Rigsbee, C. Stotz, M.J. Pikal, Dynamics of pharmaceutical amorphous solids: the study of enthalpy relaxation by isothermal microcalorimetry, J. Pharm. Sci. 91 (2002) 1853–1862.
[11] B.C. Hancock, Y. Dupuis, R. Thibert, Determination of the viscosity of an amorphous drug using thermomechanical analysis (TMA), Pharm. Res. 16 (1999) 672–675.
[12] V. Andronis, G. Zografi, Molecular mobility of supercooled amorphous indomethacin, determined by dynamic mechanical analysis, Pharm. Res. 14 (1997) 410–414.
[13] V. Andronis, G. Zografi, The molecular mobility of supercooled amorphous indomethacin as a function of temperature and relative humidity, Pharm. Res. 15 (1998) 835–842.
[14] B. Adhikari, T. Howes, B.R. Bhandari, V. Truong, Stickiness in foods: a review of mechanism and test methods, Int. J. Food Properties 4 (2001) 1–33.
[15] G.W. White, S.H. Cakebread, The glassy state in certain sugar-containing food products, J. Food Technol. 1 (1966) 73–82.
[16] Ö. Almarsson, C.R. Gardner, Novel approaches to issues of developability, Curr Drug Discov 3 (2003) 21–26.
[17] A.T.M. Serajuddin, Solid dispersion of poorly water-soluble drugs: early promises, subsequent problems, and recent breakthroughs, J. Pharm. Sci. 88 (1999) 1058–1066.
[18] R.J. Timko, N.G. Lordi, Thermal analysis of glass dispersion systems, Drug Dev. Ind. Pharm. 10 (1984) 425–451.
[19] P. Hoppu, K. Jouppila, J. Rantanen, S. Schantz, A.M. Juppo, Characterisation of blends of paracetamol and citric acid, J. Pharm. Pharmacol. 59 (2007) 373–381.
[20] R. Böhmer, K.L. Ngai, C.A. Angell, D.J. Plazek, Nonexponential relaxations in strong and fragile glass formers, J. Chem. Phys. 99 (1993) 4201–4209.
[21] K.J. Crowley, G. Zografi, The use of thermal methods for predicting glass-former fragility, Thermochim. Acta 380 (2001) 79–93.
[22] Q. Lu, G. Zografi, Properties of citric acid at the glass transition, J. Pharm. Sci. 86 (1997) 1374–1378.
[23] C.T. Moynihan, A.J. Easteal, J. Wilder, Dependence of the glass transition temperature on heating and cooling rate, J. Phys. Chem. 78 (1974) 2673–2677.
[24] G. Adam, J.H. Gibbs, On the temperature dependence of cooperative relaxation properties in glass-forming liquids, J. Chem. Phys. 43 (1965) 139–146.
[25] I.M. Hodge, Effects of annealing and prior history on enthalpy relaxation in glassy polymers. 6. Adam–Gibbs formulation of nonlinearity, Macromolecules 20 (1987) 2897–2908.
[26] C. Mao, S.P. Chamarthy, R. Pinal, Time-dependence of molecular mobility during structural relaxation and its impact on organic amorphous solids: an investigation based on a calorimetric approach, Pharm. Res. 23 (2006) 1906–1917.
[27] S. Klick, A. Sköld, Validation of a generic analytical procedure for determination of residual solvents in drug substances, J. Pharm. Biomed. Anal. 36 (2004) 401–409.
[28] R.M. Samra, G. Buckton, The crystallisation of a model hydrophobic drug (terfenadine) following exposure to humidity and organic vapours, Int. J. Pharm. 284 (2004) 53–60.
[29] M. Ueda, N. Hirokawa, Y. Harano, M. Moritoki, K. Ohgaki, Change in microstructure of an aqueous citric acid solution under crystallization, J. Cryst. Growth 156 (1995) 261–266.
[30] V. Andronis, M. Yoshioka, G. Zografi, Effects of sorbed water on the crystallization of indomethacin from the amorphous state, J. Pharm. Sci. 86 (1997) 346–351.
[31] Y. Jiugao, W. Ning, M. Xiaofei, The effects of citric acid on the properties of thermoplastic starch plasticized by glycerol, Starch/Stärke 57 (2005) 494–504.
[32] W.T. Laughlin, D.R. Uhlmann, Viscous flow in simple organic liquids, J. Phys. Chem. 76 (1972) 2317–2325.
[33] P. Sherman, Industrial Rheology with Particular Reference to Foods, Pharmaceuticals and Cosmetics, Academic Press, London, UK, 1970, p. 423.
[34] C.G. De Kruif, J.C. Van Miltenburg, A.J.J. Sprenkels, G. Stevens, W. De Graaf, H.G.M. De Witt, Thermodynamic properties of citric acid and the system citric acid–water, Thermochim. Acta 58 (1982) 341–354.
[35] E.V. Boldyreva, V.A. Drebuschak, I.E. Paukovi, Y.A. Kovalevskaya, T.N. Drebushchak, DSC and adiabatic calorimetry study of the polymorphs of paracetamol, J. Therm. Anal. Calorim. 77 (2004) 607–623.
[36] F. Xu, L.X. Sun, Z.C. Tan, J.G. Liang, T. Zhang, Adiabatic calorimetry and thermal analysis on acetaminophen, J. Therm. Anal. Calorim. 83 (2006) 187–191.
[37] P. Gupta, G. Chawla, A.K. Bansal, Physical stability and solubility advantage from amorphous celecoxib: The role of thermodynamic quantities and molecular mobility, Mol. Pharm. 1 (2004) 406–413.
[38] V.P. Privalko, Excess entropies and related quantities in glass-forming liquids, J. Phys. Chem. 84 (1980) 3307–3312.
[39] M. Goldstein, Viscous liquids and the glass transition. V. Sources of the excess specific heat of the liquid, J. Chem. Phys. 64 (1976) 4767–4774.
[40] C.A. Angell, Thermodynamic aspects of the glass transition in liquids and plastic crystals, Pure Appl. Chem. 63 (1991) 1387–1392.
[41] D. Morineau, C. Alba-Simionesco, Hydrogen-bond-induced clustering in the fragile glass-forming liquid m-toluidine: experiments and simulations, J. Chem. Phys. 109 (1998) 8494–8503.
[42] R.J. Timko, Thermal Characterization of Glass Dispersion Systems, The State University of New Jersey–New Brunswick, Rutgers, 1979 p. 197.
[43] P.I. Buler, Thermodynamic criteria of crystallization from supercooled liquid, Ceram. Int. 16 (1990) 165–169.
[44] P. Di Martino, G.F. Palmieri, S. Martelli, Molecular mobility of the paracetamol amorphous form, Chem. Pharm. Bull. 48 (2000) 1105–1108.
[45] Y. Aso, S. Yoshioka, S. Kojima, Molecular mobility-based estimation of the crystallization rates of amorphous nifedipine and phenobarbital in poly(vinylpyrrolidone) solid dispersions, J. Pharm. Sci. 93 (2004) 384–391.
[46] S.-J. Kim, T.E. Karis, Glass formation from low molecular weight organic melts, J. Mater. Res. 10 (1995) 2128–2136.
[47] B.C. Hancock, S.L. Shamblin, G. Zografi, Molecular mobility of amorphous pharmaceutical solids below their glass transition temperatures, Pharm. Res. 12 (1995) 799–806.
[48] E. Tombari, S. Presto, G.P. Johari, R.M. Shanker, Dynamic heat capacity and relaxation time of ultraviscous melt and glassy acetaminophen, J. Pharm. Sci. 95 (2006) 1006–1021.
[49] G.P. Johari, S. Kim, R.M. Shanker, Dielectric studies of molecular motions in amorphous solid and ultraviscous acetaminophen, J. Pharm. Sci. 94 (2005) 2207–2223.